Relation between surface hardening and roughness induced by ultrasonic shot peening

Julie Marteau, Maxence Bigerelle

Relation between surface hardening and roughness induced by ultrasonic shot peening

J. Marteau [a,*], M. Bigerelle [b]

[a] Laboratoire Roberval, UMR 7334, Université de Technologie de Compiègne, Centre de Recherches de Royallieu, CS 60319, 60203 Compiègne Cedex, France
[b] LAMIH, UMR 8201, Université de Valenciennes et du Hainaut Cambrésis, Le Mont Houy, F59313 Valenciennes Cedex 9, France

A B S T R A C T

This paper is focused on the identification of a relation between surface hardening and roughness induced by ultrasonic shot peening. A method that dissociates the influence of roughness from the value of the true macroscopic hardness is applied to AISI 316L stainless steel specimens treated using different processing conditions. The true macroscopic hardness is identified and used to determine the surface roughness parameter and scale that give the best relation between hardness and roughness. A relation is identified between the five point pit height S_{5V} roughness parameter (local depth of roughness) and hardness using a high-pass filter with a cut-off of 100 μm. This power function was identified at a scale that corresponds to the size of the shot impacts.

Keywords:
Multiscale roughness
Hardness
Ultrasonic shot peening
Stainless steel

1. Introduction

Hardness is an important characteristic of materials as it is part of the properties that determine tribological behaviors such as wear resistance [1] or fatigue life [2]. For instance, models were developed to estimate the strain-life curve from hardness values [3].

To improve surface properties such as hardness, different treatments are used: ion implantation [4], thermo-chemical diffusion processes such as carburization [5], mechanical processes such as shot peening [6] or laser shock peening [7]. All these treatments aim at increasing strain-hardening and compressive residual stresses. However, these surface treatments (whether they are thermal, chemical or mechanical) often give rise to surface distortion [8] or significant roughness [9]. These effects are detrimental because they promote crack nucleation and propagation [10].

Roughness can also be an obstacle to hardness determination [11–14]. Some researchers focused their investigation on the influence of surface quality on the precision of hardness calculations. Others created models to try to explain and quantify the effect of roughness on the indentation test results. For instance, Kim et al. [15] built a model assuming that the deformation of a rough material by nanoindentation is the result of the coupling of two phenomena: the flattening of the indented rough surface and the deformation of the flattened surface by nanoindentation. By analytically separating the work expended to flatten the surface from the one needed to deform the flattened surface, they developed a new indentation size effect model describing the influence of roughness. However, this model, which is based on the average surface roughness R_a, was applied with a maximum R_a approximately equal to 9 nm and was thus found to be valuable for shallow depths only.

This paper aim at investigating the relation between surface hardening and roughness induced by ultrasonic shot peening. First, a method that dissociates the effect of surface roughness from the true value of the hardness determined at the microscale, is presented and applied to ultrasonically shot peened AISI 316L specimens. Then, the identified hardness is used to find the surface roughness parameter and the scale that give the best relation between hardness and roughness. Finally, the identified relation is checked and discussed before concluding.

2. Materials and methods

2.1. Material and processing parameters

First, AISI 316L stainless steel samples were carefully polished to obtain mirror-like surfaces. Then, these samples were ultrasonically shot peened using different combinations of processing parameters. The shot diameters were equal to 1 mm or 2 mm. The shots were either made of 304L stainless steel or 100C6 steel. The vibration amplitude of the sonotrode was equal to 30 μm, 60 μm or 80 μm and the coverage (*i.e.* the percentage of the surface impacted once or more) was equal to 100%, 1000% or 10,000%. Eight specimens

* Corresponding author. Tel.: +33 3 44 23 73 34; fax: +33 3 44 23 49 84.
E-mail address: julie.marteau@utc.fr (J. Marteau).

were kept from the variation of the processing parameters in order to maximize the difference of hardness between the specimens. The specimens that are hereafter called USP_1 and USP_2 were shot using 304L balls having a diameter equal to 1 mm and 2 mm, respectively. The sonotrode vibration amplitude was set at 30 μm and the coverage was equal to 100%. USP_3 and USP_4 were treated using 30-μm vibration amplitude and 100% coverage with shots having a diameter equal to 2 mm, respectively made of 304L and 100C6. The specimens referred to as USP_5 and USP_8 are similar to USP_4 except that the vibration amplitude was set at 80 μm for the first one while the second one has a shot diameter equal to 1 mm. Similarly, USP_6 and USP_7 have the same processing conditions as USP_4 except for the coverage, which is respectively equal to 1000% and 10,000%. Table 1 summarizes the processing parameters.

2.2. Hardness measurements

One hundred instrumented indentation tests were conducted on each specimen at ambient temperature using an Agilent indenter G200, equipped with a Berkovich tip. The Continuous Stiffness Measurement (CSM) method was used with a constant strain rate equal to 0.05 s^{-1}. Fig. 1 illustrates the scattering of the loading curves, which is characteristic of rough surfaces. All the indentation curves were then prepared for the statistical treatment. To avoid any statistical artefact, three pretreatments were applied. In the first one, the loading curves are extracted from the whole load-*versus*-indentation depth curves and then truncated at 0.85 P_{max}, where P_{max} is the maximum load reached at 3 μm. The second pretreatment consists in resampling the indentation depth h in order to get an independent and identically distributed variable. The third pretreatment involves the conversion of the indentation depth h into the contact depth h_c, defined by Oliver and Pharr [16]. All the details of these pretreatments can be found in [17].

All the pretreated curves are then used to determine the hardness of each specimen through the application of the statistical model described in details in [18]. The principles underlying this statistical model are:

(i) The loading curve shapes are described using the model proposed by Bernhardt [19]:

$$P = \left\{\alpha_1 h^2 + \alpha_2 h\right\}, \tag{1}$$

where P is the load, α_1 and α_2 are constants depending on the material properties and the indenter tip geometry.
This equation corrects Kick's formula [20] through the addition of a linear term that characterizes the load dependence with increasing depth.
Eq. (1) can also be rewritten using the contact depth h_c defined by Oliver and Pharr [16]:

$$P = \alpha\left\{H_0\, h_c^2 + \beta h_c\right\} \tag{2}$$

where α is a constant depending on the geometry of the indenter, H_0 is the macrohardness of the specimen and β is the indentation size effect (ISE) factor.

(ii) Roughness disturbs the first contact detection: the indentation curves are scattered. In this method, the scatter of the experimental curves is described with the use of a relative referential: all the curves are localized according to the position of a curve chosen arbitrarily. It is assumed that the experimental curves do not fit perfectly Bernhardt's law [19]: there is a gap between the shape of a given experimental curve i and the shape predicted by Bernhardt's law [19]. This deviation from Bernhardt's law is called $\Delta h_{c,i}$.

(iii) The 100 curves per specimen are simultaneously treated in order to get an averaged H_0 and β per specimen. This simultaneous treatment enables to obtain a better representativeness.

(iv) Confidence intervals on H_0, β and $\Delta h_{c,i}$ are determined using a double Bootstrap on the 100 experimental loading curves of each specimen.

The combination of the previous points leads to the minimization of the following function:

$$\min_{H_0,\Delta h_1,\ldots,\Delta h_n,\beta} \sum_{i=1}^{n}\sum_{j=1}^{p_i}\left[P_{i,j} - \alpha\left(H_0 h_{c,j}^2 + (2H_0\Delta h_{c,i} + \beta)h_{c\,j} + H_0\Delta h_{c,i}^2 + \beta\Delta h_{c,i}\right)\right]^2, \tag{3}$$

where j refers to a point belonging to curve i.

Table 1
Processing conditions of the AISI 316L specimens.

Name	Shot material	Diameter (mm)	Sonotrode vibration amplitude (μm)	Coverage (%)
USP_1	304L	1	30	100
USP_2	304L	2	30	100
USP_3	304L	2	60	100
USP_4	100C6	2	60	100
USP_5	100C6	2	80	100
USP_6	100C6	2	60	1,000
USP_7	100C6	2	60	10,000
USP_8	100C6	1	60	100

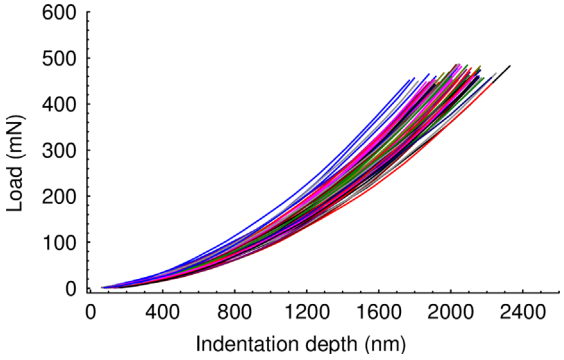

Fig. 1. Load *versus* indentation depth curves of specimen USP_5.

2.3. Roughness measurements

Surface roughness was measured using a three-dimensional non-contact optical profilometer (Zygo NewView™ 7300, Zygo Corp., USA), with a 20× objective. This configuration gave a lateral resolution equal to 710 nm and a vertical resolution of about 3 nm. Using stitching, surfaces of 1.19 mm × 0.891 mm described by 2176 × 1632 points were obtained. The stitching was realized using 10 areas of 348 μm × 262 μm with an overlapping percentage equal to 20%. For each specimen, 20 stitched surfaces were randomly measured to ensure a good representativeness of the computed roughness parameters. Finally, each surface measurement was flattened out using a polynomial of degree 3.

To describe the topography of the specimens, 50 surface roughness parameters were calculated. These parameters are:

(i) Amplitude parameters [21] such as the arithmetic mean variation S_a, the root-mean-square deviation of the surface S_q, the skewness of the height distribution S_{sk} or the kurtosis of the height distribution S_{ku}.

(ii) Functional volume parameters [22] such as the material volume V_m or the void volume V_v.

(iii) Functional parameters [23] such as the kernel roughness depth S_k or the reduced peak height S_{pk},
(iv) Hybrid parameters [21] such as the density of summits S_{ds} or the fractal dimension of the surface S_{fd},
(v) Feature parameters [22] such as the density of peaks S_{pd} or the five point valley height S_{5v}. These parameters are derived from the segmentation of a surface into motifs (*i.e.* hills and dales) thanks to the application of a watershed algorithm. This method enables to discriminate between local features (such as peaks or valleys) and larger structures (such as hills and dales). More precisely, a peak can be seen as a point on the surface which is higher than all other points within a neighborhood. A hill is the region around the peak. Similarly, a valley is a point on the surface which is lower than all other points within a neighborhood. A dale is the region around the valley. Each motif is delimited by its course line (for hills) or ridge line (for dales). The highest point of the course line of a hill and the lowest point of the course line of a dale are called a saddle point. The motif height is the height between the saddle point and the highest point of the motif (*i.e.* the peak) for a hill while it is the height between the lowest point of the motif (*i.e.* the pit) and the saddle point for a dale. Examples of 3D roughness measurements and their corresponding motifs are given in Fig. 2.

Surface topography is examined using a multiscale analysis involving the use of different cut-off filters and cut-off lengths. More specifically, a total of 50 surface roughness parameters were evaluated using two types of robust Gaussian filter (low-pass or high-pass) [24] over 21 cut-off lengths. These different parameters enabled to emphasize specific features of the surfaces. For instance, Fig. 3 illustrates the motifs that can be obtained when filtering the roughness measurements presented in Fig. 2 with a high-pass filter and different cut-off lengths. It can be seen that depending on the chosen cut-off length, very different motifs are obtained. These different segmentations give very different roughness parameter values, as shown in Fig. 4. More details are provided on the topography of the studied specimens in [25], which describes the link between the processing conditions and the obtained morphology.

To provide a confidence interval for each surface roughness parameter associated with a cut-off length and a filter, the bootstrap theory was applied. This statistical theory consists in generating a large number of simulated samples by randomly sampling with replacement the set of experimental values. This technique is thoroughly described in [26].

2.4. Method for assessing the relations between roughness and hardness

The search for a relation between hardness and roughness was made using the simulated bootstrap values. For a given roughness parameter, type of filter (*i.e.* low-pass or high-pass) and cut-off length, a relation was searched between the roughness values and the hardness values. To do so, four types of functions mixing linear and logarithmic parts were used: a linear–linear model, a logarithmic–logarithmic model, a linear–logarithmic model and a logarithmic–linear model. The relation giving the best coefficient of determination was selected as the best model.

3. Results and discussion

3.1. Indentation test results

First, the deviation Δh_c, which stands for the gap between the experimental curve shape and the one described by Bernhardt's law, is calculated for each specimen by minimizing the function given in Section 2.2. Fig. 5 shows the histograms of the Δh_c values associated with their standard deviations for the reference specimen (USP_0) and the ultrasonically shot peened specimens (USP_1 to USP_8).

Overall, the histograms of the specimens have a Gaussian shape. Only the specimen called USP_7 tends to deviate from this trend as a discretization effect appears. This discretization is due to the small number of load-indentation depth curves used to build this graph. Indeed, all the experimental curves were not used because some of them presented large breaks in their slope due to high roughness. Removing the latter from the 100 experimental curves led to use only 30 curves, thus giving rise to the discretization effect. However, this discretization effect could be removed either by increasing the number of curves used in the calculation, or by using the kernel bandwidth optimization method.

The specimen used as a reference (USP_0) has the smallest standard deviation of Δh_c, which is approximately equal to 28 nm. The specimen showing the largest standard deviation (151 nm) is USP_7. The other treated specimens show standard deviations ranging from 40 nm to 72 nm.

The different values found for the standard deviations are probably an evidence of the effect of the roughness amplitude on the deviation of the indentation curves. To assess this effect, the standard deviation of Δh_c is represented as a linear function of the root-mean-square roughness of the surface S_q, using simple linear regression. This relation is evaluated using different cut-off lengths in order to determine the scale at which the best fit is obtained. The relevance of the slope is assessed by examining the value of the '*t*' statistic, hereafter called $S_{q,\Delta}$ (a significant value means that the slope is not zero). Fig. 6 depicts the relevance of the slope of this linear relation as a function of the cut-off length. The best relevance is found for a cut-off length approximately equal to 15 μm. As indicated by Fig. 7, it gives a linear relation between the standard deviation of the deviation Δh_c and the root-mean-square roughness S_q having a coefficient of determination equal to 0.94.

This proportionality proves that the extent of the deviations Δh_c is directly linked to the roughness amplitude. The best relation between both parameters was found using a scale equal to 15 μm, which is of the order of magnitude of the indentation imprints.

The minimization of the function given in Section 2.2 also enables to calculate the macrohardness of each specimen, associated with their distributions. The distribution of each macrohardness H_0 also has a bell curve shape, as illustrated by Fig. 8. This bell curve shape is characteristic of a Gaussian distribution. The specimen showing the largest scatter of data is specimen USP_7, too. Globally, the specimens show significantly different hardness values. With an average value of 3.5 GPa, the reference specimen (USP_0) has the lowest hardness. Specimens USP_2, USP_3, USP_1 and USP_4 have an average hardness equal to 4.2 GPa, 4.3 GPa, 4.4 GPa and 4.5 GPa, respectively. The specimens called USP_5 and USP_8 show similar results: they have an average hardness equal to 4.9 GPa, with nearly identical distributions. Specimens USP_6 and USP_7 have the highest hardness values with averages equal to 5.3 GPa and 5.7 GPa, respectively.

Finally, the minimization also enables to determine a single ISE factor β for each specimen. The ISE factor is an important parameter as it enables to characterize the indentation size effect taking place in the material and more precisely, the occurrence of pile-up. Indeed, as reported in [27], a positive ISE factor reflects the occurrence of pile-up. Fig. 9 depicts the ISE factor values calculated for the reference specimen as well as for the ultrasonically shot peened specimens. The median values all lie between 1000 and 2200 mN/nm, thus indicating the occurrence of pile-up. To confirm this result, the indentation imprints were observed with a scanning electron microscope. A clear pile-up can

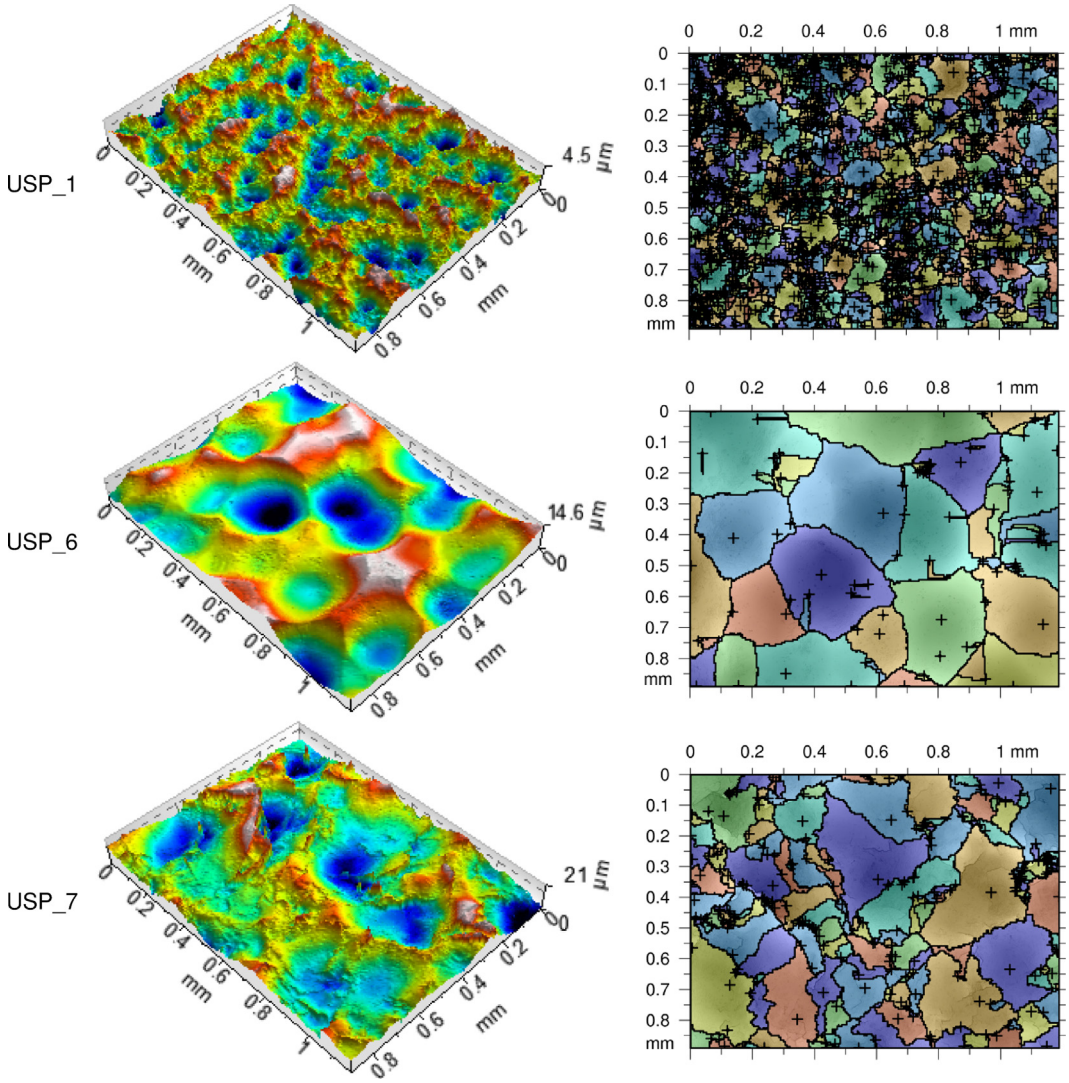

Fig. 2. 3D roughness measurements and corresponding motifs for specimens USP_1, USP_6 and USP_7.

be observed when the specimens are tilted with an angle of 65°, as illustrated by Fig. 10.

3.2. Relation between roughness and hardness

In the previous section, it was shown that the difference of shapes between the experimental loading curves and the ones predicted by Bernhardt's model was proportional to the variation of roughness when the latter is calculated over a scale of the size of the indentation imprints (15 μm). Taking into account this deviation and the indentation size effect, a true and accurate value of the macrohardness H_0 was determined for each specimen. As previously discussed, all the specimens show distinct hardness values. These values could be linked to surface roughness.

In order to assess the relation between the hardness of the ultrasonically shot peened specimens and their topography, the simulated bootstrap values of different roughness parameters are expressed as a function of the simulated bootstrap values of hardness. As indicated in Section 2.4, for each roughness parameter, four types of relations were evaluated between the hardness values and the roughness values, at different scales using a combination of cut-off filters and cut-off lengths. These combinations gave rise to the evaluation of approximately 10,000 relations or models, assessed using the value of their coefficient of determination. The best correlation between the surface roughness of the specimens and the hardness values was found using a power law and the five point valley height S_{5V} roughness parameter calculated using a high-pass filter. The identified relation was then assessed over different cut-off lengths in order to determine the most relevant scale, as shown in Fig. 11. This curve has a unique maximum, approximately located at a cut-off length equal to 100 μm.

The coupling of the previous findings indicate that the best coefficient of determination is equal to 0.73 and is found when the hardness values are expressed as a power function of five point valley height, S_{5V}, roughness parameter. As depicted in Fig. 12, the following equation is identified:

$$H_0 = 2.8\{S_{5V} + 2.71\}^{0.31} \quad (4)$$

It is important to note that this model was built using only the ultrasonically shot peened specimens. Thus, the experimental hardness values calculated for the reference specimen can be used to test the validity of this model. Indeed, when the value of the valley height parameter is set to zero in Eq. (4), the power law should be able to predict the experimental hardness. As shown in Fig. 13, Eq. (4) predicts an average macrohardness H_0 equal to equal to 3.7 GPa with a standard deviation equal to 0.3 GPa. Experimentally, the macrohardness was found to be equal to

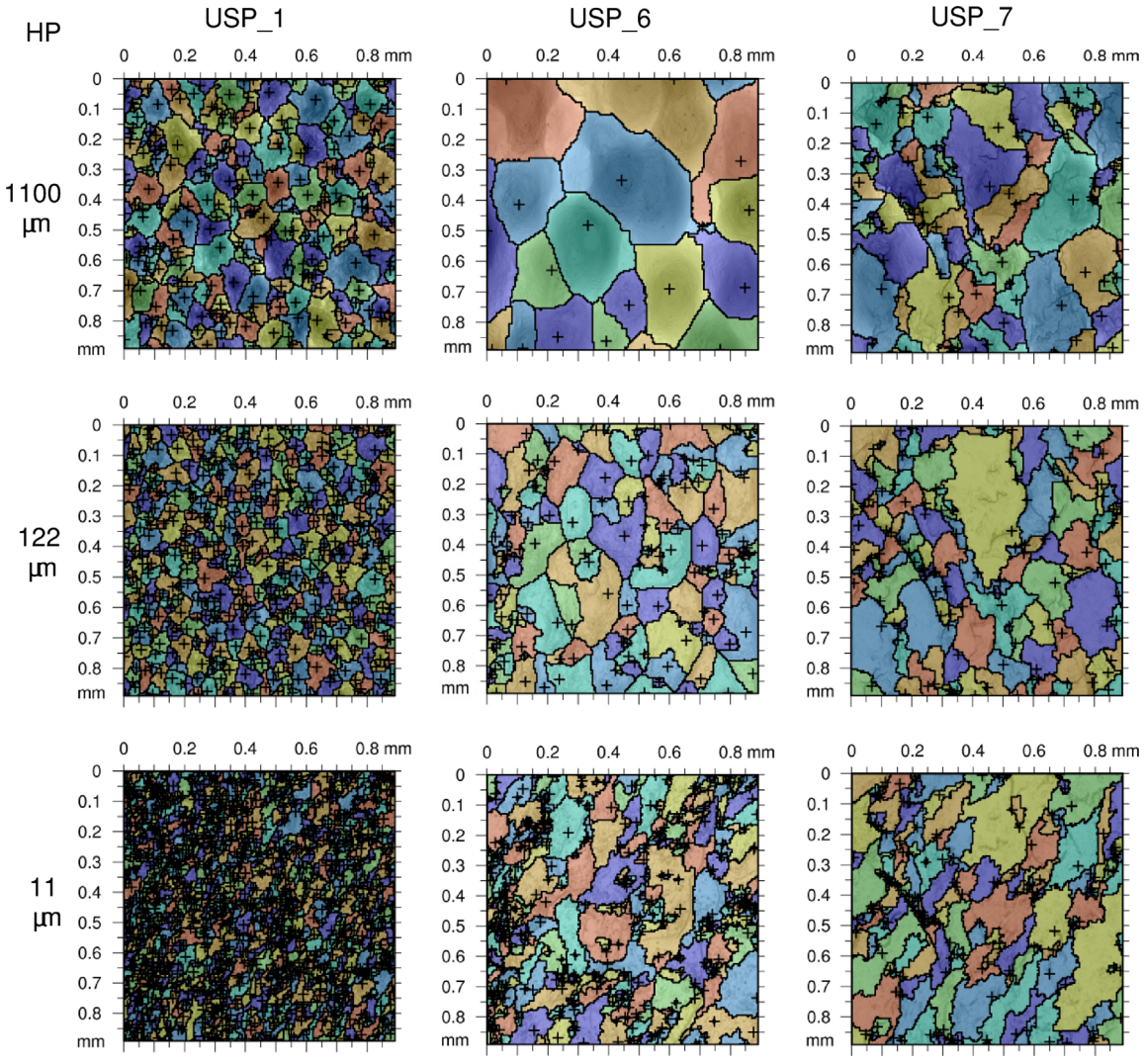

Fig. 3. Motifs of specimens USP_1, USP_6 and USP_7, calculated using a high-pass filter (HP) and cut-off lengths equal to 11 µm, 122 µm and 1100 µm.

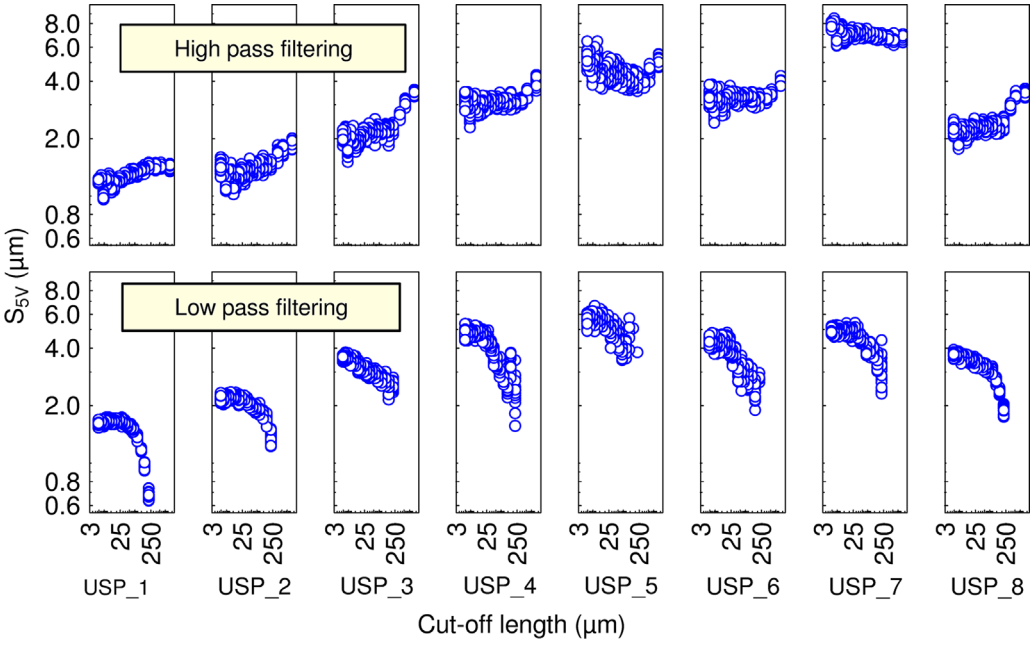

Fig. 4. The 5-point valley height S_{5V} roughness parameter as a function of the cut-off length, using high-pass and low-pass filters, for the eight ultrasonically shot peened specimens.

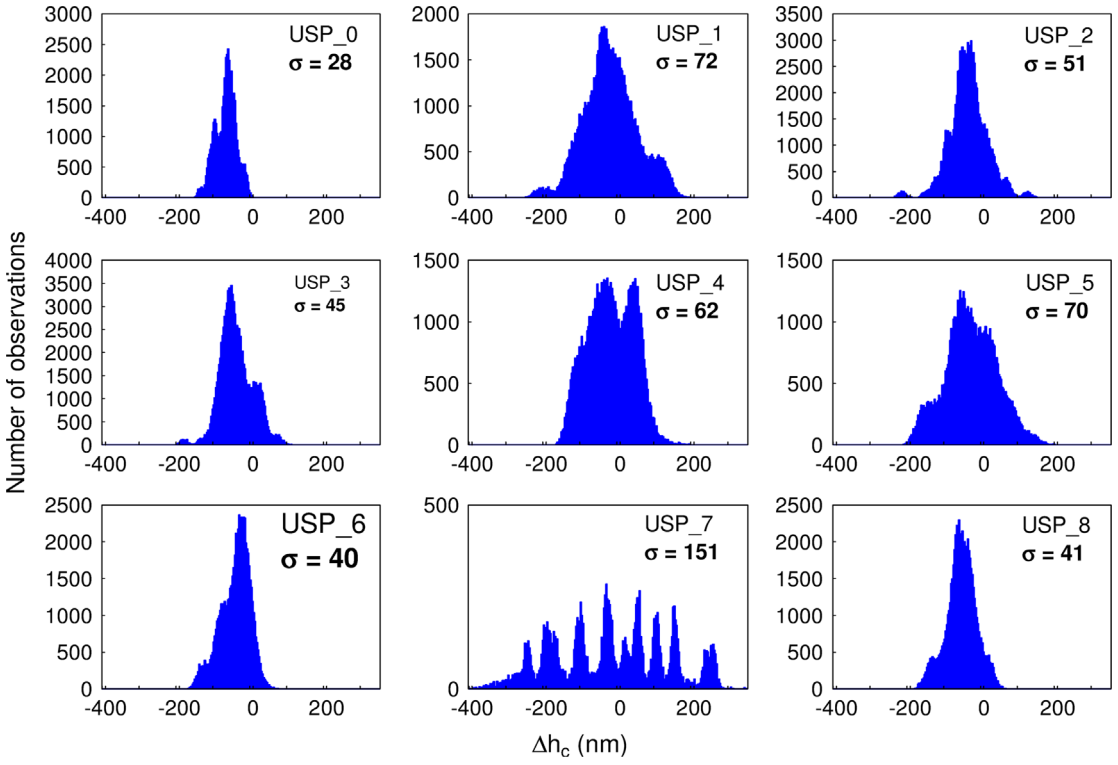

Fig. 5. Histograms of the deviations Δh_c between the experimental curve shape and the one predicted by Bernhardt's law, for the reference specimen and the eight ultrasonically shot peened specimens.

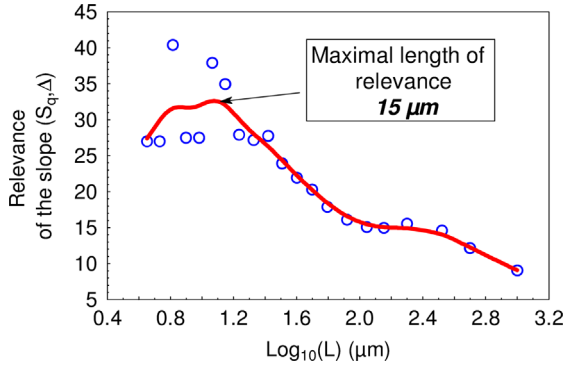

Fig. 6. Relevance of the slope of the linear relation between the standard deviation of the gaps Δh_c and the root-mean square roughness S_q parameter of the surface as a function of the cut-off length L.

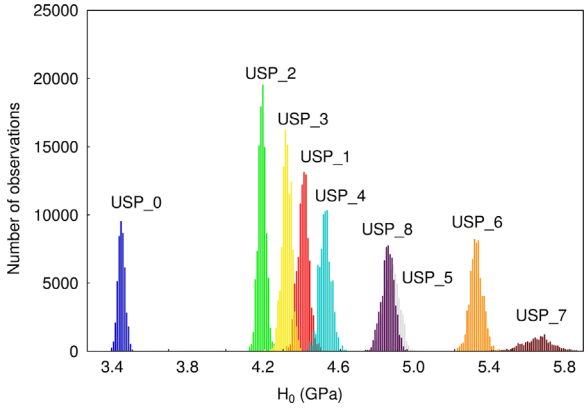

Fig. 8. Distributions of the macrohardness H_0 values for the reference specimen and the eight ultrasonically shot peened specimens.

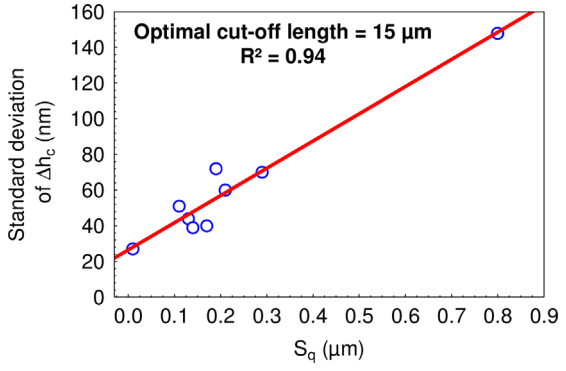

Fig. 7. Evolution of the standard deviation of the gaps Δh_c as a function of the Root-Mean Square S_q roughness parameter.

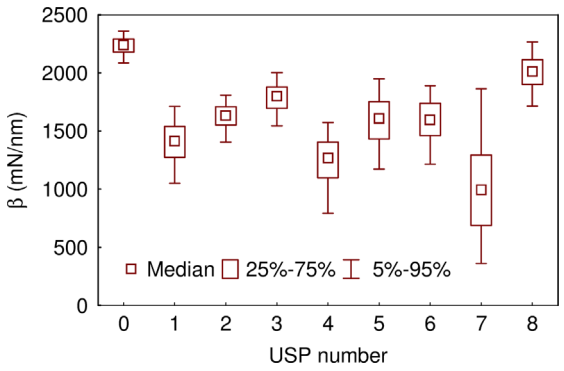

Fig. 9. Medians and standard deviations calculated for the ISE factor β for the reference specimen and the eight ultrasonically shot peened specimens.

3.48 ± 0.02 GPa for the reference specimen. The latter belongs to the interval predicted by the model, thus confirming the predictive power of the model.

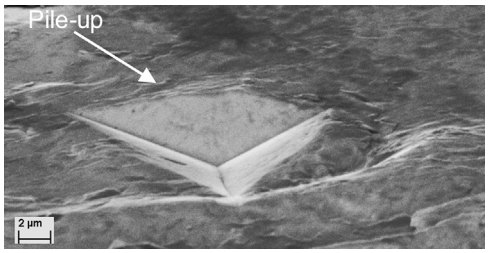

Fig. 10. Image of an indentation imprint of Specimen USP_7. The image was taken with a scanning electron microscope and a tilt angle of 65°.

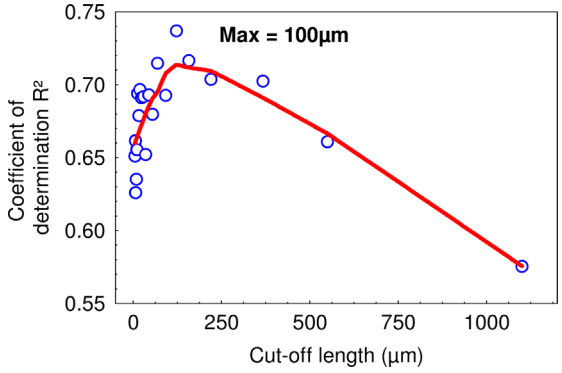

Fig. 11. Evolution of the coefficient of determination R^2 as a function of the cut-off length.

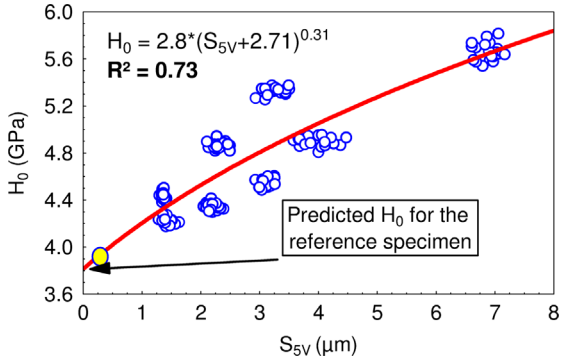

Fig. 12. Evolution of the macrohardness H_0 as a function of the 5-point valley height S_{5V} roughness parameter.

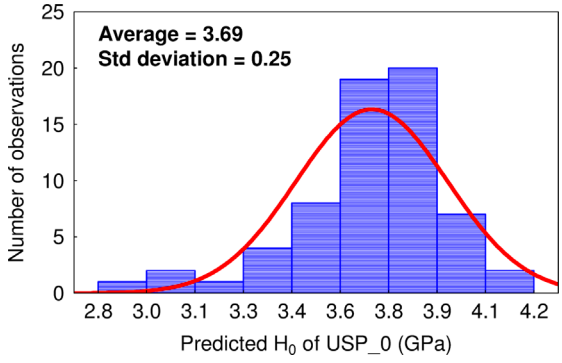

Fig. 13. Histogram of the macrohardness H_0 values of the reference specimen, predicted by the model described by Eq. (4).

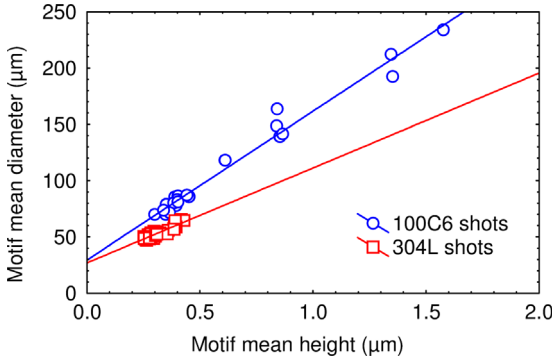

Fig. 14. Mean height of the motifs as a function of the mean diameter of the motifs, calculated using a high-pass filter and a cut-off length equal to 100 µm, for the specimens called USP_3 (304L shots) and USP_4 (100C6 shots).

It should be noted that Eq. (4) has a form equivalent to one of the most commonly used behavior law: Krupkowski's law. The latter is used to describe the plastic behavior of isotropic metallic materials. This law is described by the following equation:

$$\sigma = \sigma_y + K\{\varepsilon_p + \varepsilon_0\}^n, \tag{5}$$

where σ is the stress, σ_y is the yield stress, ε_p is the plastic strain, ε_0 is the initial strain and K and n are constants. This law is similar to Ludwig's equation, except that a possible pre-deformation of the material is taken into account. According to Tabor [28], the hardness of metallic materials is approximately equal to three times the yield stress of the material. Giving this proportionality, the relation described by Eq. (4) can be seen as a prediction of the yield stress of the material after the ultrasonic shot peening treatment, as follows:

$$\sigma_y = \frac{2.8}{3}\{S_{5V} + 2.71\}^{0.31} \tag{6}$$

Thus, the measurement of the valley height could give some indication on the material properties. Furthermore, the valley height is probably itself linked with the ball impacts. It would thus give a direct relation between the ball penetration and the material yield stress.

The five-point valley height S_{5V} parameter is directly based on the size of the calculated motifs (*cf.* Fig. 3). Thus, to confirm a possible relation between the valley height parameter and the ball impacts, the motifs obtained with a high-pass filter and a cut-off length equal to 100 µm were studied. Fig. 14 shows the mean height of the motifs of the specimens USP_3 and USP_4 as a function of the diameter of the motifs. It can be seen that a height equal to 0.3 µm corresponds to a motif diameter ranging from 50 µm to 60 µm. To a first approximation, the indent caused by the penetration of a shot can be described as follows:

$$d^2 = 4uD, \tag{7}$$

where u is the indent depth, D is the shot diameter and d is the indent diameter. For an indent depth equal to 0.3 µm and a shot diameter equal to 2 mm, this formula predicts an indent diameter approximately equal to 50 µm. This good agreement between the predicted diameter and real motif diameter confirms that the valley height is directly linked with the shot impacts. The measured motif diameter and the calculated indenter diameter are of the same order of magnitude as the cut-off length used to find Eq. 4. It thus seems that the latter is found at a scale corresponding to the ball impacts.

To further confirm the developed model and the identified scale, the autocorrelation length was calculated for all the treated specimens, as shown in Fig. 15. This parameter provides spatial

information on surface topography: it calculates the length at which the surface is correlated with itself. Roughly speaking, it can be used as a mathematical tool to characterize the length at which the profile "loses its memory". To compare different topographies, the maximum autocorrelation length should be chosen to avoid losing information. Here, the maximum is found for USP_5 and is approximately equal to 90 μm. This length is of the same order of magnitude as the cut-off length used to find Eq. 4: it thus confirms that the best relation between roughness and hardness is found at a scale corresponding to the size of the shot impacts.

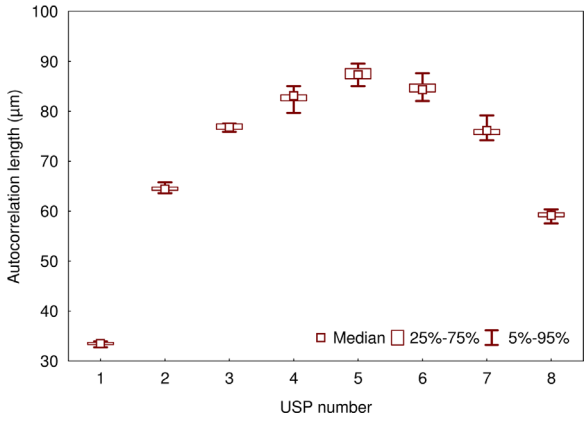

Fig. 15. Medians and standard deviations of the autocorrelation lengths calculated for the eight ultrasonically shot peened specimens.

4. Conclusion

In this paper, the simultaneous study of topography and hardness enabled to identify a relation between surface hardening and roughness induced by shot peening. The methodology and different results are summarized in Fig. 16.

First, a novel methodology enabling to dissociate hardness from surface effects was presented and applied to ultrasonically shot peened specimens. Using different processing parameters, it was shown that the material hardness can be identified despite large roughness. The indentation size effect was also characterized and was found to be the same, irrespective of the processing parameters. It was also shown that the Root-Mean-Square roughness and the standard deviation values of zero-point corrections show a clear linear relation at the scale of the indentation imprints (15 μm), thus confirming previously found results.

Using calculated hardness values, the best relation between hardness and roughness was searched for ultrasonically shot peened specimens, testing several surface roughness parameters computed using different filters and cut-off lengths. It was found that the five-point valley height S_{5V} parameter calculated using a high-pass filter with a cut-off length of 100 μm gives the best relation between roughness and hardness for ultrasonically shot peened specimens. The cut-off length of 100 μm also corresponds to the size of the shot impacts, thus further confirming the relevance of the identified relation. Finally, it was shown that the identified relation accurately predicts the roughness of the reference specimen, thus bearing out the model.

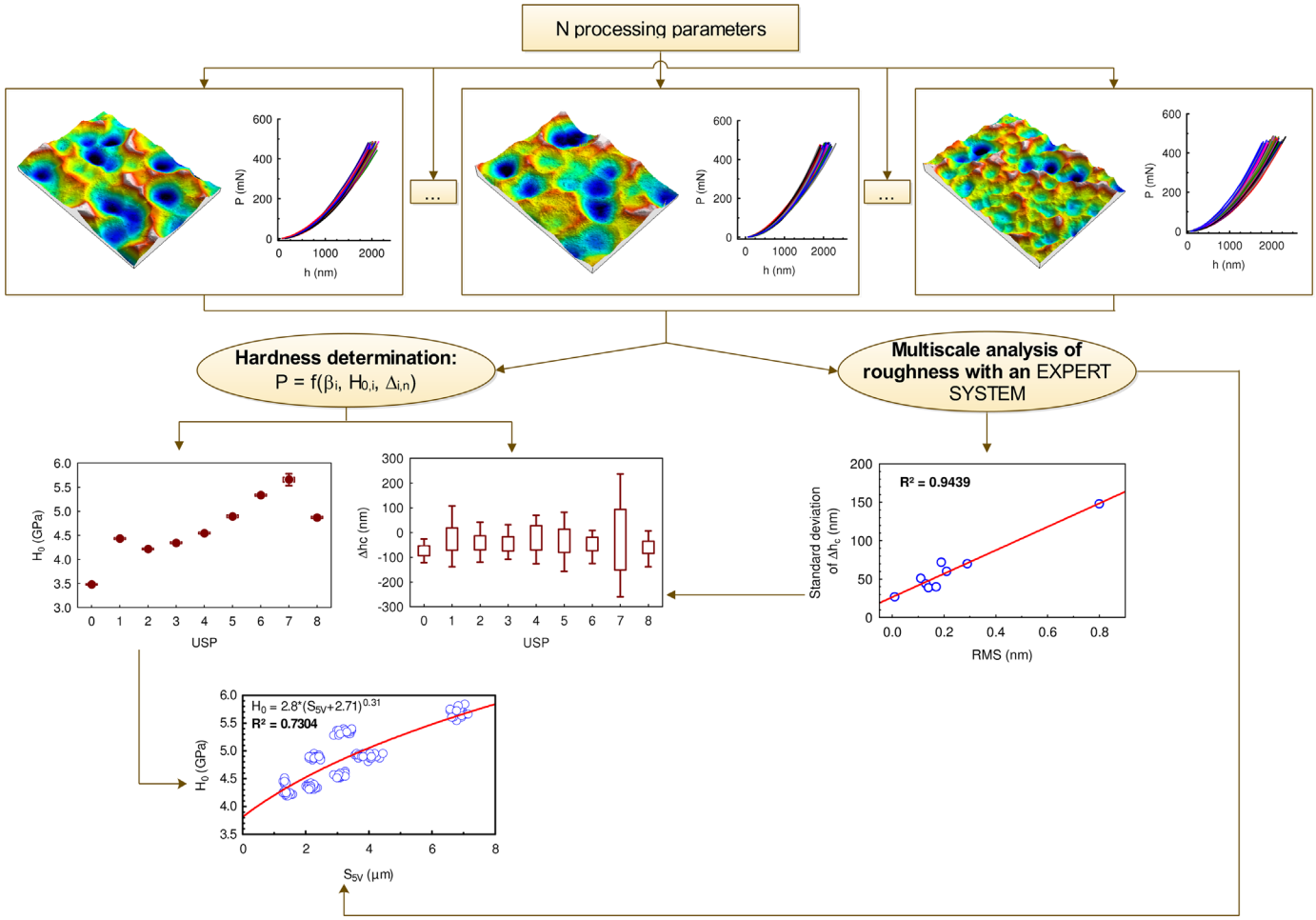

Fig. 16. Graphical summary of the methodology used for the examination of the link between surface hardening and roughness induced by ultrasonic shot peening.

References

[1] Viáfara CC, Sinatora A. Influence of hardness of the harder body on wear regime transition in a sliding pair of steels. Wear 2009;267:425–32.
[2] Wu H, Hamada S, Noguchi H. Fatigue strength prediction for inhomogeneous face-centered cubic metal based on Vickers hardness. Int J Fatigue 2013;48:48–54.
[3] Roessle ML, Fatemi A. Strain-controlled fatigue properties of steels and some simple approximations. Int J Fatigue 2000;22:495–511.
[4] Cai Z-b Zhang G-a, Zhu Y-k Shen M-x, Wang L-p, Zhu M-h. Torsional fretting wear of a biomedical Ti6Al7Nb alloy for nitrogen ion implantation in bovine serum. Tribol Int 2013;59:312–20.
[5] Cao Y, Ernst F, Michal GM. Colossal carbon supersaturation in austenitic stainless steels carburized at low temperature. Acta Mater 2003;51:4171–81.
[6] Heredia S, Fouvry S, Berthel B, Panter J. A non-local fatigue approach to quantify Ti–10V–2Fe–3Al fretting cracking process: application to grinding and shot peening. Tribol Int 2011;44:1518–25.
[7] Srinivasan S, Garcia DB, Gean MC, Murthy H, Farris TN. Fretting fatigue of laser shock peened Ti–6Al–4V. Tribol Int 2009;42:1324–9.
[8] Farrell K, Specht ED, Pang J, Walker LR, Rar A, Mayotte JR. Characterization of a carburized surface layer on an austenitic stainless steel. J Nucl Mater 2005;343:123–33.
[9] Bagherifard S, Ghelichi R, Guagliano M. Numerical and experimental analysis of surface roughness generated by shot peening. Appl Surf Sci 2012;258:6831–40.
[10] Curtis S, de los Rios ER, Rodopoulos CA, Levers A. Analysis of the effects of controlled shot peening on fatigue damage of high strength aluminium alloys. Int J Fatigue 2003;25:59–66.
[11] De Souza GB, Lepienski CM, Foerster CE, Kuromoto NK, Soares P, Ponte HdA. Nanomechanical and nanotribological properties of bioactive titanium surfaces prepared by alkali treatment. J Mech Behav Biomed Mater 2011;4:756–65.
[12] Li M, Chen W, Cheng Y-T, Cheng C-M. Influence of contact geometry on hardness behavior in nano-indentation. Vacuum 2009;84:315–20.
[13] Bobji MS, Shivakumar K, Alehossein H, Venkateshwarlu V, Biswas SK. Influence of surface roughness on the scatter in hardness measurements—a numerical study. Int J Rock Mech Min Sci 1999;36:399–404.
[14] Qasmi M, Delobelle P. Influence of the average roughness Rms on the precision of the Young's modulus and hardness determination using nanoindentation technique with a Berkovich indenter. Surf Coat Technol 2006;201:1191–9.
[15] Kim J-Y, Kang S-K, Lee J-J, Jang J-i, Lee Y-H, Kwon D. Influence of surface-roughness on indentation size effect. Acta Mater 2007;55:3555–62.
[16] Oliver WC, Pharr GM. An improved technique for determining hardness and elastic modulus using load and displacement sensing indentation experiments. J Mater Res 1992;7:1564–83.
[17] Marteau J, Mazeran PE, Bouvier S, Bigerelle M. Zero-point correction method for nanoindentation tests to accurately quantify hardness and indentation size effect. Strain 2012;48:491–7.
[18] Marteau J, Bigerelle M, Xia Y, Mazeran PE, Bouvier S. Quantification of first contact detection errors on hardness and indentation size effect measurements. Tribol Int 2013;59:154–62.
[19] Bernhardt EO. On microhardness of solids at the limit of Kick's similarity law. Z Metallkd 1941;33:135–44.
[20] Kick F. Das Gesetz der proportionalen Widerstände und seine Anwendungen: Nebst Versuchen über das Verhalten verschiedener Materialien bei gleichen Formänderungen sowohl unter der Presse als dem Schlagwerk: Verlag von Arthur Felix; 1885.
[21] Stout KJ, Matthia T, Sullivan PJ, Dong WP, Mainsah E, Luo N, et al. The developments of methods for the characterisation of roughness in three dimensions. Report EUR 15178 EN1993.
[22] Standardization IOf. ISO standard 25178. International Organization for Standardization; 2012.
[23] Standardization IOf. ISO standard 13565. International Organization for Standardization; 1996.
[24] Standardization IOf. ISO standard TS 16610-31. International Organization for Standardization; 2010.
[25] Marteau J, Bigerelle M, Mazeran PE, Bouvier S. Relation between roughness and processing conditions of AISI 316L stainless steel treated by ultrasonic shot peening. Tribol Int.
[26] Najjar D, Bigerelle M, Iost A. The computer-based bootstrap method as a tool to select a relevant surface roughness parameter. Wear 2003;254:450–60.
[27] Iost A, Bigot R. Indentation size effect: reality or artefact? J Mater Sci 1996;31:3573–7.
[28] Tabor D. The hardness of metals. USA: Oxford University Press; 1949.